

## Plant species' spectral emissivity and temperature using the hyperspectral thermal emission spectrometer (HyTES) sensor

Susan Meerdink<sup>a,\*</sup>, Dar Roberts<sup>b</sup>, Glynn Hulley<sup>c</sup>, Paul Gader<sup>a</sup>, Jan Pisek<sup>d</sup>, Kairi Adamson<sup>d</sup>, Jennifer King<sup>b</sup>, Simon J. Hook<sup>c</sup>

<sup>a</sup> Civil and Coastal Engineering Department, University of Florida, Gainesville, FL 32611, United States of America

<sup>b</sup> Department of Geography, University of California Santa Barbara, Santa Barbara, CA 93106-4060, United States

<sup>c</sup> National Aeronautics and Space Administration Jet Propulsion Laboratory, Pasadena, CA 91109, United States

<sup>d</sup> University of Tartu, Tartu Observatory, 61602 Tõravere, Estonia



### ARTICLE INFO

#### Keywords:

Thermal infrared  
Spectral emissivity  
Plant species  
Land surface temperature (LST)  
HyTES  
Remote sensing  
Hyperspectral  
Random forest

### ABSTRACT

The thermal domain (TIR; 2.5–15 μm) delivers unique measurements of plant characteristics that are not possible in other parts of the electromagnetic spectrum. However, these TIR measurements have largely been restricted to laboratory leaf level or coarse spatial resolutions due to the lack of suitable data from airborne and spaceborne instruments. The airborne Hyperspectral Thermal Emission Spectrometer (HyTES) provides an opportunity to retrieve high spectral resolution emissivity and land surface temperature (LST) that can be exploited for canopy level vegetation research. This study is a high spatial resolution analysis of plant species' emissivity and LST using HyTES imagery acquired in the Huntington Botanical Gardens on 2014 July 5 and 2016 Jan 25. Leaf and canopy emissivity variation was identified among 24 plant species and used to determine leaf to canopy scaling capabilities. HyTES LST patterns among species and dates were quantified and correlated to LiDAR derived tree canopy attributes. At the leaf scale, one third of the species showed distinct spectral separation from other species. However, at the canopy scale most species were not spectrally separable. Random forest classification demonstrates the high level of confusion between species with overall accuracies < 40%. LST data, derived from TIR measurements, showed that species exhibited significantly different distributions between dates and species. These distributions were largely explained by canopy structure (e.g. tree height and canopy density) and composition of neighboring pixels (e.g. presence of pavement versus trees). While species do not exhibit unique emissivity signatures at the canopy level, the LST variation among species provides a stronger understanding of LST variability in coarser resolution TIR imagery. This study represents the analysis of vegetation characteristics using the NASA's HyTES TIR sensor, opening the door for future remote sensing vegetation studies that include using the recently launched ECOSTRESS mission.

### 1. Introduction

The thermal infrared (TIR; 2.5–15 μm) domain affords two unique measurements of plant characteristics through emissivity and land surface temperature (LST) that are not possible using the visible-shortwave infrared spectrum (0.35–2.5 μm). These measurements are being used for vegetation research at multiple scales including the determination of leaf water content (Fabre et al., 2011; Ullah et al., 2012b), plant evaporation rates (Anderson and Kustas, 2008; Otkin et al., 2014), and large-scale drought monitoring (Kogan, 1995a; Liu and Kogan, 1996). The increased availability of TIR sensors and technological advances has now made it increasingly possible to examine

vegetation characteristics using emissivity and LST measurements.

TIR emissivity signatures are unique from the visible-shortwave infrared because of how light interacts with the leaf. Due to the low energy of TIR wavelengths, leaves appear opaque because energy does not penetrate leaf surfaces (Gates and Tantraporn, 1952; Salisbury, 1986; Salisbury and Milton, 1988). Measured spectral emissivity for a leaf is the product of light interactions with the outer layers of the leaf (Elvidge, 1988; Salisbury, 1986; Wong and Blevin, 1967). In contrast, spectra in the visible-shortwave infrared domain are the product of light interactions with the internal leaf structure and biochemical components because the high energy wavelengths of this domain can penetrate leaf surfaces (Curran, 1989). Ribeiro da Luz (2006)

\* Corresponding author.

E-mail address: [susanmeerdink@ufl.edu](mailto:susanmeerdink@ufl.edu) (S. Meerdink).

conducted one of the first studies to investigate vegetation characteristics in the TIR and found that leaves display complex absorption features related to organic constituents of leaf surfaces. Since then, high spectral resolution TIR laboratory measurements have been leveraged to quantify leaf water content using a variety of methods (Arshad and Ali, 2018; Buitrago et al., 2016; Fabre et al., 2011; Meerdink et al., 2016; Ullah et al., 2014, 2013, 2012b). Other studies have leveraged this domain for plant species classification at the leaf level (Buitrago et al., 2018; Harrison et al., 2018; Ullah et al., 2012a) or leaf area index estimation (Neinavaz et al., 2016). These studies demonstrate the successful application of TIR emissivities for the study of leaf characteristics, but with the caveat that these relationships may not translate to canopy scale and are only relevant for high spatial resolution sensors at the few meter scale.

Ultimately, to address the broader science and remote sensing questions, it is necessary to scale these studies to the canopy. Ribeiro Da Luz and Crowley (2007) were the first ones to address this knowledge gap by making measurements at increasing distances from natural canopies with a field spectrometer. Other studies have also used high spectral resolution TIR imaging under controlled laboratory conditions to measure canopy changes due to water stress (Gerhards et al., 2016) and to develop a relationship with leaf area index (Neinavaz et al., 2016). Ribeiro Da Luz and Crowley (2010) provide the only study, to our knowledge, that has used airborne hyperspectral TIR imagery to study plant characteristics. Using Spatially-Enhanced Broadband Array Spectrograph System (SEBASS; Hackwell et al., 1996) imagery, the research identified spectral differences between species located in the State Arboretum of Virginia. TIR emissivity measurements at the canopy level have been few in number due to lack of sensors and low signal to noise ratios of the available sensors.

TIR LST measurements are unique because of the relationship between plant temperatures and plants' response to the environment. As plants close stomata to maintain their carbon-water balance, plant temperatures increase due to a decrease in evapotranspiration rates (Jones, 2014). This relationship has long been recognized in plant ecology and used as an indicator of plant water relations and stress (Calderón et al., 2013; Grant et al., 2007; Jackson et al., 1988; Jones and Leinonen, 2003; Sepulcre-Cantó et al., 2006). Leaf or field level LST measurements have been used for developing irrigation and crop health indices (Fuchs, 1990; Fuchs and Tanner, 1966; Jackson et al., 1981, 1977; Jones and Leinonen, 2003; Jones and Schofield, 2008), estimating stomatal conductance (Jones, 1999; Jones et al., 2002; Leinonen et al., 2006), calculating evapotranspiration rate (Anderson et al., 2008; Fisher et al., 2008), or measuring an evaporative stress index (Anderson et al., 2016; Otkin et al., 2014, 2013). Satellite level LST measurements have been used for global or regional drought monitoring (Kogan, 1995b; Liu and Kogan, 1996; Singh et al., 2003).

While these studies have successfully used temperature as a proxy for plant water status, many other factors can influence a plant's canopy temperature. Leuzinger and Körner (2007) found that leaf dimensions and stomatal conductance alone could not capture canopy temperatures and that canopy architecture has a strong influence on canopy LSTs. Additionally, the presence or absence of key taxa or plant functional types influences the temperature distribution of a forest and an urban environment (Leuzinger et al., 2010; Leuzinger and Körner, 2007). In these studies, leaf type (broad vs. needle), leaf size (small vs. large), and substrate (grass vs. concrete) interacted to create unique temperature distributions and sensitivity among tree species (Leuzinger et al., 2010, 2005; Leuzinger and Körner, 2007). Our understanding of plant LST patterns are especially limited at the canopy level, mainly due to the coarse spatial resolution of satellite measurements and the lack of plant structural variability available in agricultural field measurements.

The Hyperspectral Thermal Emission Spectrometer (HyTES) is a recent sensor developed using new technologies from the National Aeronautics and Space Administration (NASA) Jet Propulsion Laboratory (JPL). This sensor presents a unique opportunity to study

vegetation properties at the canopy level with a 2 m spatial resolution at a nominal flight altitude of 1 km. HyTES measures 256 radiance bands in the 7.5–12 μm spectral domain at 17 nm spectral sampling (Hook et al., 2013). High spatial resolution (2–10 m) temperature and emissivity data are currently available to order from <https://hytes.jpl.nasa.gov/order> for science campaigns over the Southwestern USA and Hawaii from 2013 to 2018. Using a temperature emissivity separation algorithm developed by JPL, this sensor is able to retrieve the land surface temperatures and spectral emissivity for 186 bands in the TIR window region between 8 and 12 μm (Hook et al., 2013). This sensor has been used in a variety of research projects including methane/trace gas detection and quantitative retrievals (Hulley et al., 2016; Johnson et al., 2014; Kuai et al., 2016) and geological composition (Iqbal et al., 2018; Kruse, 2015). High spectral resolution and fine spatial resolution TIR imagery has not been widely used for vegetation due to the lack of suitable measurements and the subtle features of plants (Ribeiro Da Luz and Crowley, 2010). However, the HyTES sensor presents an opportunity to examine canopy properties at these resolutions.

The purpose of our study was to explore the possibility of using HyTES imagery for measuring plant species' canopy characteristics. HyTES's 186 TIR emissivity bands provide a unique opportunity to study patterns of TIR canopy signatures that were previously only possible with a limited number of sensors (e.g. SEBASS). The high accuracy LST retrievals at fine spatial resolutions allow for the examination of patterns across species and dates. We investigate drivers of LST variability using LiDAR derived canopy attributes. Specifically, we asked the following questions:

- 1) What TIR spectral variation among plant species is present at the leaf scale?
- 2) Using HyTES imagery, do plant species exhibit unique TIR emissivity signatures at the canopy scale?
- 3) How do LST patterns vary among species, canopy attributes, and dates?

## 2. Methods

### 2.1. Study site

The Huntington Botanical Gardens, located in San Marino, CA, USA, is a collections-based research and educational institution established in 1919 (Fig. 1). It covers approximately 48.6 ha and contains about 15,000 documented plant varieties, most of which are tagged and identified. In order to best relate laboratory spectra to canopy spectra, plants with canopies having at least a 12-meter diameter were identified using a database provided by the Huntington Gardens, high-resolution imagery, and field assessment. Out of these species, 24 species with three or more individuals were selected (Table 1). Each selected individual identified had fresh leaf samples taken for laboratory measurements (see Section 2.2). Only tree canopies with a diameter larger than 12 m were chosen for this analysis to ensure there were multiple pixels for each individual tree. The polygons of individual trees were used to extract emissivity and LST values from HyTES imagery (see Section 2.3) and also LiDAR variables (see Section 2.5). Only pixels completely falling into a reference polygon were used to avoid the edge of tree canopies. The number of pixels differed between image sources due to different spatial resolutions. Table 1 lists the 24 plant species sampled in this study with the number of pixels associated for each with 2014 and 2016 imagery.

### 2.2. Leaf measurements

Fresh leaf samples were harvested in the field, and spectral measurements were conducted in the laboratory. Samples were collected on February 2, October 3, and October 6, 2016. Samples were collected from tree species using pole clippers and from shrub species using

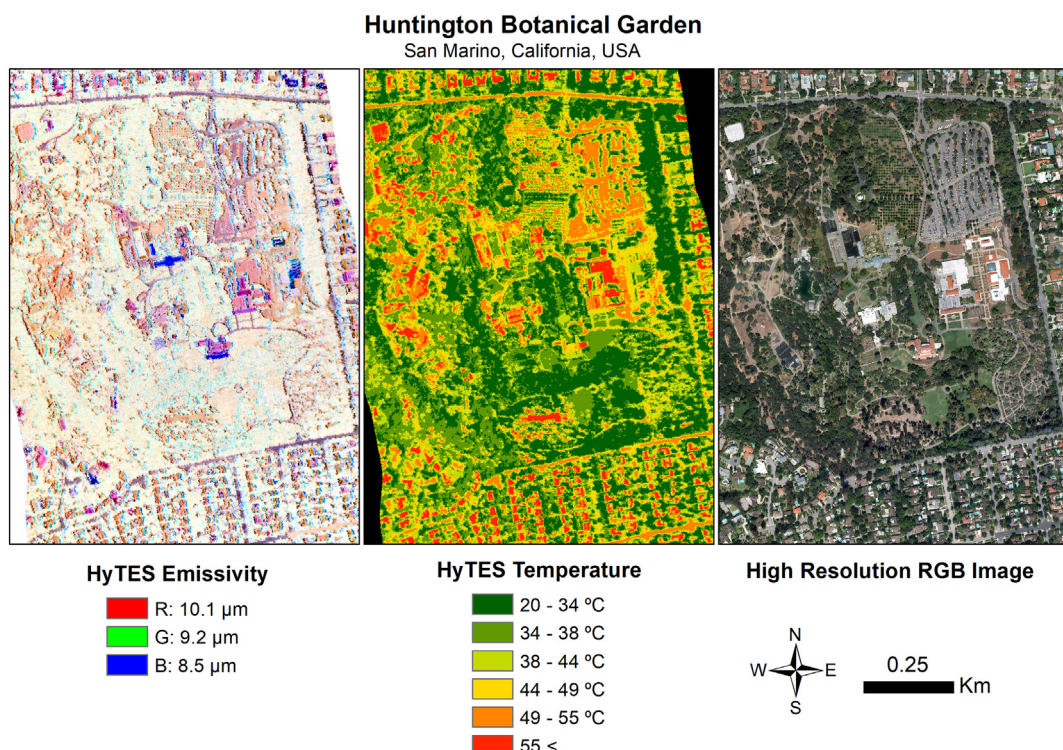


**Fig. 1.** HyTES imagery at 2 m resolution (1100 AGL flight altitude) from 2014 July 5 showing emissivity (left panel) and Land Surface Temperature (LST; middle panel). Emissivity is displayed with bands 10.1  $\mu$ m as red, 9.2  $\mu$ m as green, and 8.5  $\mu$ m as blue. Right panel shows high spatial resolution RGB imagery of the Huntington Gardens study area in San Marino, California, USA. (For interpretation of the references to colour in this figure legend, the reader is referred to the web version of this article.)

pruning shears. Multiple leaves were collected from individual plants, with leaves randomly selected from the highest accessible part of the canopy. For taller individuals this means that sampled leaves received full sun for part of the day, whereas leaf samples from shorter individuals were collected from the top of the canopy in full sun exposure. The leaves were wrapped in damp paper towels and placed in

polyethylene bags to be stored in a cooler at  $\sim$ 10 °C with a towel to prevent direct contact with ice. In order to preserve the integrity of the samples, spectra were measured at the NASA JPL within 48 h of collection.

Before spectral analysis, leaves were removed from polyethylene bags and excess moisture was wiped off. If a single leaf did not fill the

**Table 1**  
Summary of plant species sampled in this study with associated sample sizes.

Plant species	Acronym	Common name	N for nicolet	N for HyTES 2014	N for HyTES 2016
<i>Aloe arborescens</i>	ALAR	Candelabra Aloe	3	23	24
<i>Bambusa beecheyana</i>	BABE	Beechey Bamboo	6	35	44
<i>Bambusa tuldaoides</i>	BATU	Punting Pole Bamboo	3	42	44
<i>Brachychiton discolor</i>	BRDI	Lacebark	3	52	58
<i>Brachychiton rupestris</i>	BRRU	Queensland Bottle	3	37	53
<i>Caesalpinia cacaia</i>	CACA	Cascalote	3	20	30
<i>Cassia leptophylla</i>	CALE	Golden Medallion	3	40	42
<i>Cedrus deodara</i>	CEDE	Deodar Cedar	3	43	53
<i>Chorisia insignis</i>	CHIN	White Silk Floss	3	34	36
<i>Chorisia speciosa</i>	CHSP	Silk Floss	3	40	45
<i>Ficus columnaris</i>	FICO	Moreton Bay Fig	3	32	38
<i>Ficus thonningii</i>	FITH	Stranger Fig	3	46	53
<i>Jacaranda mimosifolia</i>	JAMI	Jacaranda	3	30	34
<i>Lagerstroemia indica</i>	LAIN	Crape Myrtle	3	47	55
<i>Magnolia grandiflora</i>	MAGR	Southern Magnolia	3	39	46
<i>Melaleuca linariifolia</i>	MELI	Snow-in-summer	3	38	42
<i>Peltophorum africanum</i>	PEAF	Weeping Wattle	3	35	37
<i>Podocarpus gracilior</i>	POGR	Fern Pine	3	57	65
<i>Quercus agrifolia</i>	QUAG	Coast Live Oak	3	65	80
<i>Quercus ilex</i>	QUIL	Holly Oak	3	31	40
<i>Quercus robur</i>	QURO	English Oak	3	27	34
<i>Quercus suber</i>	QUSU	Cork Oak	3	24	25
<i>Quercus virginiana</i>	QUVI	Southern Live Oak	3	41	49
<i>Salix babylonica</i>	SABA	Weeping Willow	3	45	53
<i>Tipuana tipu</i>	TITI	Tipu	3	42	54

laboratory spectrometer field of view, multiple leaves from the same individual were clustered while minimizing gap and overlap between leaves. Leaves were placed on aluminum foil to minimize background effects that may be present from gaps. A Nicolet 520FT-IR Spectrometer fitted with a Labsphere gold coated integrating sphere (model RSA N1 700D) was used to measure reflectance from 2.5 to 15.4  $\mu\text{m}$  (Thermo Electron Corp., Madison, WI, USA). This sensor uses a single EverGlo infrared light source that has a bulb temperature of 1140 °C to output constant radiation. To reduce the impact of moisture in the air on the spectra, dry air was sent into the external sphere. Gold was measured once every hour and used as a standard to calibrate the Nicolet spectrometer. Distilled water was used to check the calibration and accuracy of reflectance products. The Nicolet spectrometer has a sampling interval of 0.001  $\mu\text{m}$ , and each spectrum was determined from 300 scans, which took approximately 3 min to collect. Each plant sample was an average of three spectra, which were collected in one of two ways. First, a single set of leaves was measured and rotated three times. Second, three sets of different leaves from the same individual were measured.

Nicolet spectrometer spectra also underwent quality assurance through visual assessment and were averaged using code located at <https://github.com/susanmeerding/ASD-Nicolet-Spectra-Processing>. Measurements were used to calculate emissivity by using Kirchhoff's Law ( $\epsilon = 1 - R$ ), which in turn, enables comparisons to be made between the laboratory spectral measurements and HyTES emissivities images. The uncertainty associated with the Nicolet FT-IR emissivities is 0.002 (0.2%). Measurements were then convolved to HyTES bands using a Gaussian model with a 0.1  $\mu\text{m}$  full width half maximum (FWHM) and HyTES band center wavelengths that ranged from 8.3 to 11  $\mu\text{m}$  (Hook et al., 2013). Examples of leaf emissivities resampled to HyTES wavelengths are shown in Fig. 2 with all species shown in Fig. S1 and S2. All references to leaf emissivities in this paper refer to the ones resampled to HyTES wavelengths.

### 2.3. Canopy measurements and temperature emissivity separation

HyTES is a hyperspectral airborne sensor that measures radiance across 256 bands in the 7.5–12  $\mu\text{m}$  spectral range (Hook, Johnson, & Abrams, 2013). The HyTES sensor was flown on the Twin Otter plane on two dates: 2014 July 5 and 2016 January 25 (Fig. 1). The HyTES sensor can be flown at various altitudes above the ground surface that provides the flexibility to obtain data at different spatial resolutions. The 2014 flightline was flown at 17h42m UTC with a spatial resolution

of 1.7 m, and the 2016 flightline was flown at 22h36m UTC with a spatial resolution of 1.9 m. Air temperatures during flights were 31 °C and 22 °C for July 2014 and January 2016, respectively. Humidity during flights were ~40% and ~30% for July 2014 and January 2016, respectively. Examples of canopy emissivities from 2014 and 2016 are shown in Fig. 2 and all species are shown in Fig. S1 and S2.

Deriving Land Surface Temperature (LST) and spectral emissivity from HyTES is an underdetermined problem since there are more unknowns (256 band emissivities, 1 temperature) than the total number of measurements available (256 radiances). To solve the underdetermined problem, HyTES uses an adapted version of the Temperature Emissivity Separation (TES) algorithm (Gillespie et al., 1998) initially developed for the ASTER 5-band thermal infrared (TIR) radiometer. TES is typically used for multispectral sensors with three or more bands in the TIR so that spectral variations in the retrieved emissivity can be related to surface composition and cover, in addition to retrieving the LST. TES is currently used to retrieve standard LST and emissivity products for ASTER, the Moderate Resolution Imaging Spectroradiometer (MODIS) (Hulley and Hook, 2011), the Visible Infrared Imager Radiometer Suite (VIIRS) (Islam et al., 2017), and the ECOSystem Spaceborne Thermal Radiometer Experiment on Space Station (ECOSTRESS) thermal sensors with accuracies at the 1 K level for globally representative surfaces (Malakar and Hulley, 2016). The constraint used in TES for solving the problem is based on an empirical relationship that predicts the minimum emissivity ( $\epsilon_{min}$ ) from the observed radiance spectral contrast, or minimum-maximum emissivity difference (MMD) for the set of bands being used (Kealy and Hook, 1993; Matsunaga, 1994). Other hyper- and multi-spectral temperature/emissivity separation approaches include the iterative spectrally smooth temperature emissivity separation method (ISSTES) and other variations of ISSTES based on different smoothing criteria (Borel, 2008; Cheng et al., 2010), and rely on the constraint that emissivity features are smooth across atmospheric absorption spectral features. However, while variations of this method may work in theory, they rely heavily on near perfect atmospheric correction and well calibrated data with low noise levels. For these reasons the TES algorithm combined with a modified elevation-dependent In-Scene Atmospheric Correction (ISAC) clustering approach yielded the most accurate and stable results for the HyTES instrument (Hulley et al., 2016) with uncertainties at the 1.5–2 K level (2–3% in emissivity) on average for a range of different land surface types (Hook et al., in press). The major advantage of the ISAC method is that atmospheric correction is accomplished using the hyperspectral data itself without the need for external atmospheric profiles or radiative

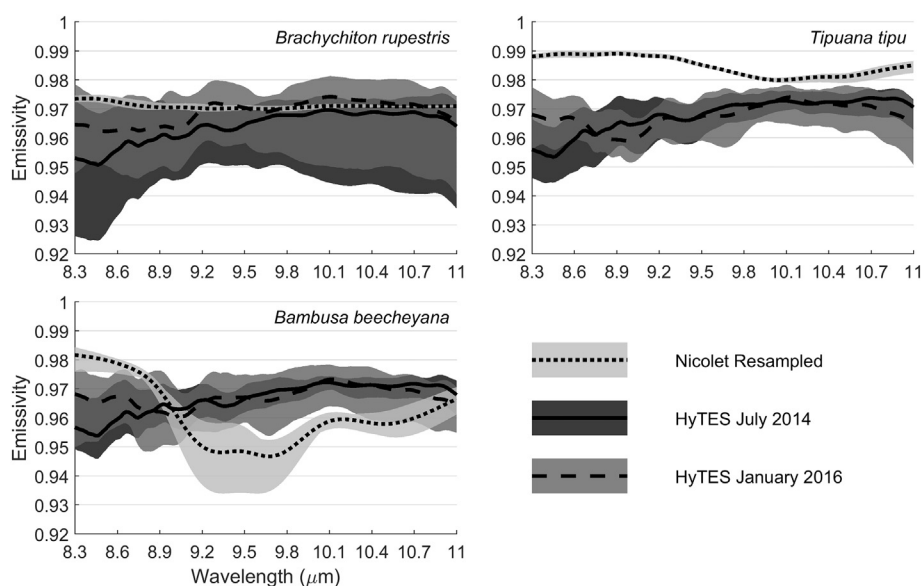


**Fig. 2.** Emissivities of three select species from three sources: Leaf emissivities resampled from Nicolet spectrometer, canopy emissivity from July 2014 HyTES imagery, and canopy emissivity from January 2016 HyTES imagery. Shaded areas designate the minimum and maximum emissivity measured. Other species are shown in Figs. S1 and S2.

transfer models, thereby eliminating the issue of spectral band misregistrations (Young et al., 2002). Of the 256 bands of HyTES, the TES-ISAC approach is used to retrieve spectral emissivity for 186 clear window channels between 8.2 and 11  $\mu\text{m}$ . Channels below 8.2  $\mu\text{m}$  are avoided due to strong water vapor absorption features in this spectral domain, while channels above 11  $\mu\text{m}$  are discarded due to issues with calibration of the instrument. More details and specifics of the HyTES L2 TES-ISAC algorithm are available in an algorithm theoretical basis document (ATBD) upon request.

#### 2.4. Spectral analysis and classification

Mann-Whitney *U* Test (MWU), also known as the Wilcoxon Test, was used to determine significant differences in species pairs because the distributions of emissivities were non-parametric. MWU is performed at each wavelength comparing species pairs' emissivities and is summarized in two ways: per wavelength and per species pair. For each wavelength, we report the total number of species pairs that were significantly different from a single species' emissivity distribution. This identifies wavelengths where a species is significantly unique from the 23 other species analyzed. For each species pair, we report the total number of wavelengths that are significantly different. This identifies which species are more spectrally similar or dissimilar from each other. In addition, species separability was tested using spectral angle mapper (SAM) which calculates the spectral angle between two spectral vectors that have a common origin (Kruse et al., 1993). SAM measures differences in spectral shape across all wavelengths, while MWU measures differences in emissivity at a single wavelength. The statistical difference in species LST distributions was analyzed using ANOVA.

In order to fully determine plant separability based on emissivity, random forest classification was conducted on the July 2014 and January 2016 datasets. The random forest classifier was executed in MATLAB software package (The MathWorks, Natick, Massachusetts, USA). For each species, 80% of samples were randomly selected for training, while the remaining 20% were used for validation. Fifty iterations of randomly selecting training, classifying, and validating were completed for each of the HyTES image dates. The random forest classification was run with the number of variables to be selected as the square root of the number of input variables, and the number of decision trees was set to 500 (Belgiu and Dragut, 2016). Confusion matrices from the random forest classification show results using the total number of validation samples across the fifty iterations.

#### 2.5. LiDAR imagery

Light Detection and Ranging (LiDAR) terrain data were collected over the Huntington Gardens in 2014 through the Los Angeles Region Imagery Acquisition Consortium (LARIAC4; *LARIAC Product Guide 2006–07*, 2006). The spatial resolution is 10.2 cm with vertical accuracy of 27.7 cm at a 95% confidence level. Multiple LiDAR products were used to derived canopy structural attributes and properties (Table 2). Polygons of individual trees, described in Section 2.1, were used to extract tree height statistics, including mean, maximum, minimum, standard deviation, and range of heights. These polygons were also used to extract the total number of returns for a tree canopy and calculate tree canopy size. To determine a tree's neighbors, the LARIAC4 land cover classification product was used. This product has an overall accuracy of 97.86% with seven land cover classes, including tree, grass/shrub, bare soil, water, buildings, roads/railroads, and other pavement. The water and building classes were not included because < 2% of trees had these classes as neighbors. A 5-meter buffer around tree individuals was used to extract the surrounding land cover pixels to determine tree neighbors. Information derived from the LiDAR products was summarized for each individual and correlated with mean, maximum, and minimum canopy LSTs.

### 3. Results

#### 3.1. Leaf emissivity

Spectral angles identified separability between the plant species pairs for leaf emissivities based on spectral shape (Fig. 3a). Among the most spectrally distinct were two species from the *Bambusa* family (BABE and BATU), which are known to have strong silica content expressed as a strong absorption feature. Other notable species that were distinct with spectral angles above 0.1 rad included QURO and FITH. However, most species pairs had relatively small spectral angles even at the leaf level, demonstrating that spectral shapes between species are too similar for separability.

While spectral angle determines separability based on spectral shape, Mann-Whitney-U (MWU) tests determine separability based on the number of wavelengths containing significantly different emissivities. For MWU tests, the majority of species pairs had > 75% of wavelengths exhibit significantly different emissivities (Fig. 4a). Among the most spectrally distinct species were CEDE, PEAF, POGR, and TITI. This analysis also can determine which species might be spectrally confused with each other. For example, POGR was spectrally distinct from most species, but not from PEAF and QUIL. Other species, such as ALAR and CEDE, were not spectrally distinct from most, but compared to a single species had > 75% significantly different wavelengths.

Another aspect of MWU analysis is the ability to determine which wavelengths contain the largest discriminating power for plant species (Fig. 5a; Fig. S3–S5). At the leaf level, the 24 species are categorized into three groups: a) species that were spectrally different between 8.3 and 11  $\mu\text{m}$ ; b) species that were spectrally different for a subset of wavelengths; or c) species that were not spectrally distinct. There were three species (CEDE, POGR, TITI) that were spectrally distinct from other species across the measured TIR spectrum. Eight species (BABE, BATU, BRRU, CALE, FICO, FITH, MAGR, and PEAF) had portions of their emissivities that were distinct from other species. For example, BABE was similar to 20% of the species pairs in the 4–6  $\mu\text{m}$  range, but was similar to 80% of the species pairs between 8 and 10  $\mu\text{m}$ . However, the majority of species fell into the final category where their emissivities were not spectrally distinct in the 2.5–11  $\mu\text{m}$  range. These species, such as SABA and ALAR, had emissivities that were the least separable with only 10–20% significant pairs.

#### 3.2. Canopy emissivity

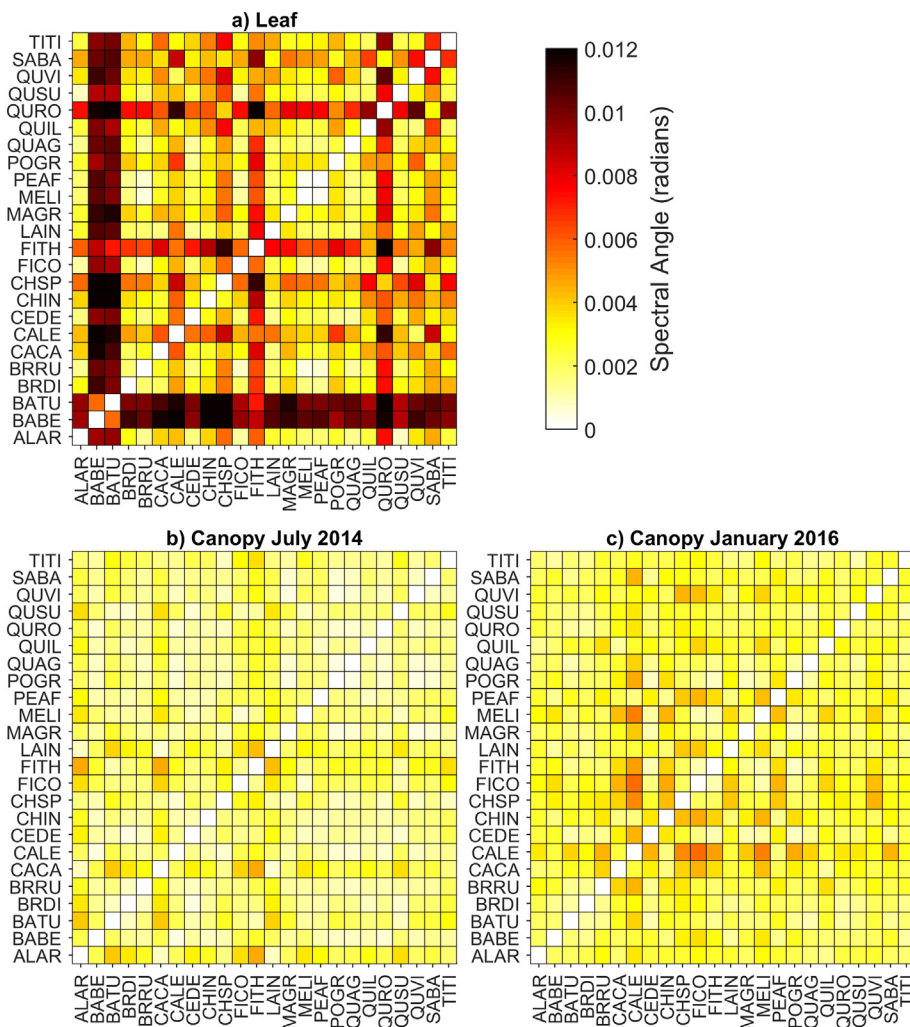
Canopy emissivities were significantly different from laboratory leaf emissivities for most wavelengths of the 24 species in July 2014 and January 2016 (Fig. 6). In general, species' emissivities at the leaf and canopy were least similar between 9.9 and 10.5  $\mu\text{m}$ . Across 8.3–11  $\mu\text{m}$ , at least 12 of the 24 species were significantly different between leaf and canopy emissivities. These 12 species had canopy attributes that are known to decrease the ability to retain leaf spectral information at the canopy. One of those species, TITI, commonly has an open canopy which will increase the influence of substrate in canopy emissivity. BABE has canopies composed of diverse leaf orientations which retain less spectral information due to multiple scattering that occurs in canopies. However, there were some species with canopy emissivities more similar to measured leaf emissivities. For example, CHIN and CHSP had 73% of wavelengths that were spectrally similar between the two levels. These two species were broadleaf planophile trees, which are able to retain leaf spectral information due to favorable geometries. Leaf emissivities for these species might be representative of canopy emissivities for portions of the TIR. However, for most species, leaf emissivities were not representative of canopy emissivities. Leaf level could not be directly translated to canopies without additional scaling algorithms.

Separability of species based on spectral shape was very low for both of the canopy emissivity dates compared to leaf emissivities

**Table 2**

Descriptive and statistical metrics extracted from LiDAR data.

	Variable name	Variable description
Height above ground	Mean	Mean height above ground for a tree canopy
	Min	Minimum height above ground for a tree canopy
	Max	Maximum height above ground for a tree canopy
	Std	Standard deviation of height above ground for a tree canopy
Neighbors	Range	Range of heights above ground for a tree canopy
	Other trees	Number of pixels classified as trees within 5 m buffer of tree canopy
Other	Grass/shrub	Number of pixels classified as grass/shrub within 5 m buffer of tree canopy
	Bare soil	Number of pixels classified as bare soil within 5 m buffer of tree canopy
	Roads	Number of pixels classified as roads within 5 m buffer of tree canopy
	Other pavement	Number of pixels classified as other pavement within 5 m buffer of tree canopy
	Tree size	Tree canopy size ( $m^2$ )
Other	Num. of returns	The total number of returns for a tree canopy

**Fig. 3.** The spectral angle between species for emissivities collected from (a) leaf resampled to HyTES wavelengths, (b) canopy July 2014, and (c) canopy January 2016 imagery.

(Fig. 3b & 3c). Spectral angles showed that January 2016 canopy emissivities had slightly more separation between species, but separability was marginal. For both dates, spectral angles between species pairs were consistently low, with only a couple of species in 2016 (CALE and PEAF) showing more separability with higher spectral angles across dates. The smaller spectral angles observed for canopy emissivities compared to leaf emissivities demonstrate that the spectral

variability among species observed at the leaf scale did not translate to the canopy.

Analyzing the number of wavelengths that were significantly different between species pairs reveals a similar pattern at the canopy level (Fig. 4b & c). Compared to leaf spectra, both dates had a higher number of species pairs with only 0–50% of wavelengths being significantly different at the canopy level. While leaf emissivities only had

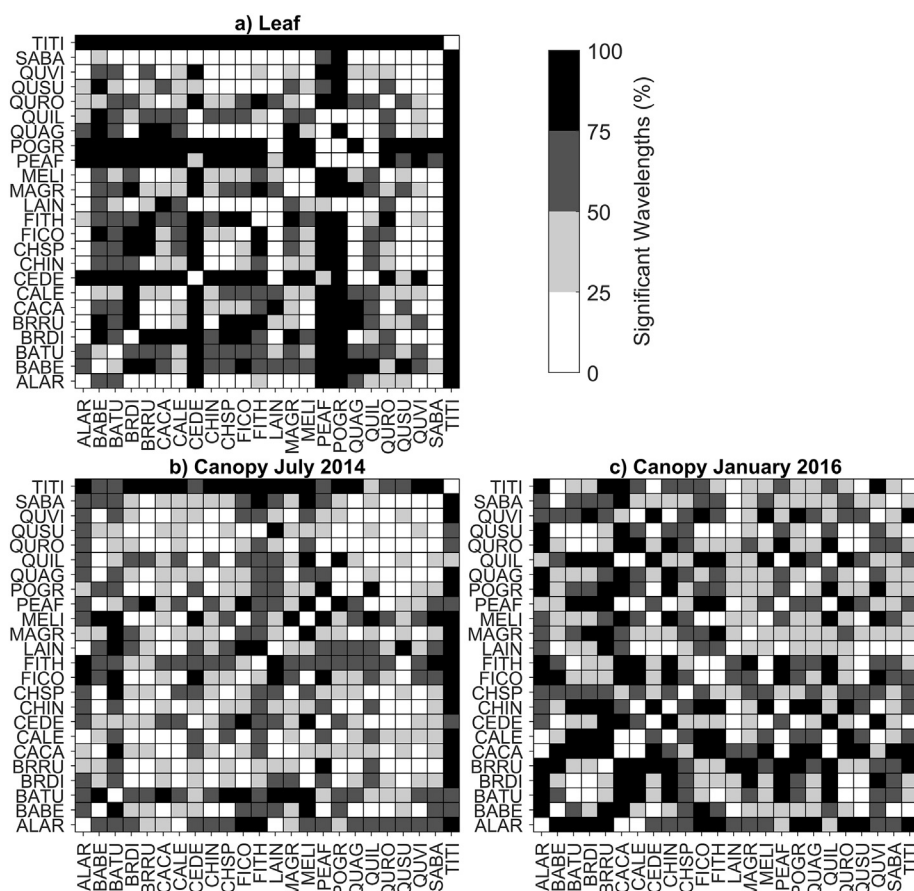


**Fig. 4.** The percent of wavelengths that are significantly different ( $p < 0.05$ ) between species pairs for (a) leaf emissivity resampled to HyTES wavelengths, (b) canopy July 2014 emissivity, and (c) canopy January 2016 emissivity.

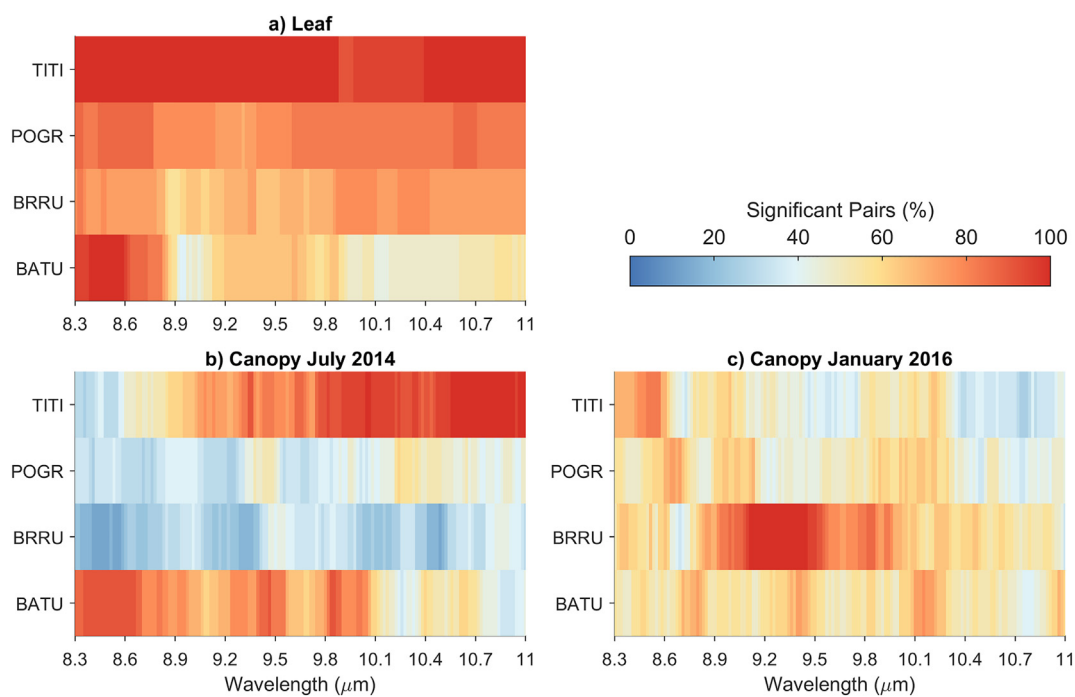


**Fig. 5.** The percent of significantly different pairs at each wavelength identified by Mann Whitney U (MWU) tests for plant species emissivities from the (a) leaf resampled to HyTES wavelengths, (b) canopy July 2014, and (c) canopy January 2016. For other species' significant wavelengths, see Figs. S3–S5.

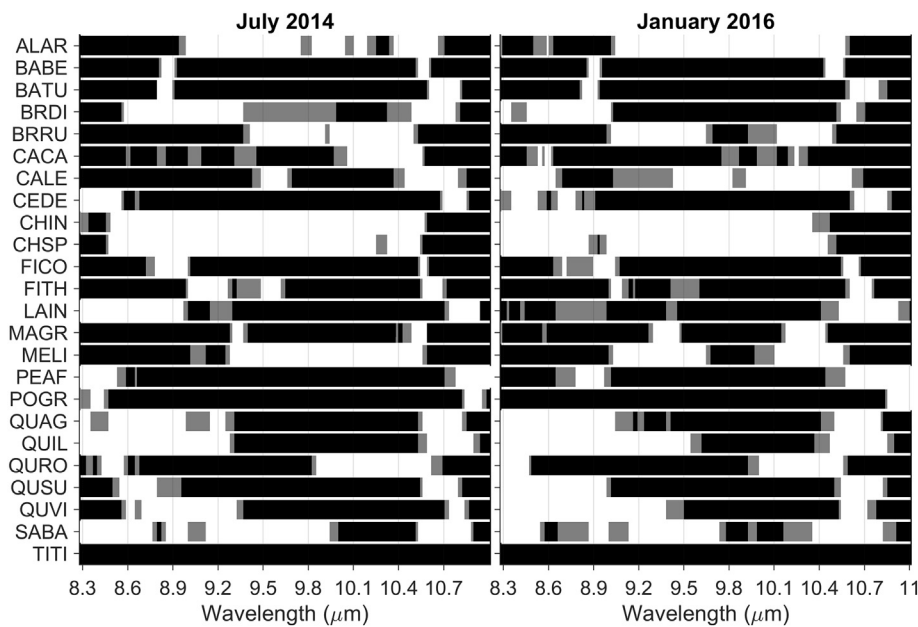


**Fig. 6.** Wavelengths that were significantly different between leaf emissivities and canopy emissivities from 2014 (left) and 2016 (right). Gray designates wavelengths at significance of  $p < 0.05$  and black designates significance at  $p < 0.01$ .

129 pairs in this low distinguishability category, July 2014 had 170 pairs and January 2016 had 145 pairs emphasizing that many species became more spectrally similar when scaled to the canopy. This analysis also highlights seasonality differences when separating species spectrally. In general, canopy emissivities were more spectrally distinct in January 2016 than July 2014. Some species pairs, such as ALAR and TITI, remained spectrally distinct from each other over the two time periods while most experienced changes in separability strength.

Similar to leaf emissivities, species exhibited different sets of influential wavelengths at the canopy level, which shifted between the two image dates (Fig. 5b & c). However, unlike leaf emissivities, no species were spectrally distinct for the entire 8.3–11  $\mu\text{m}$  range. The majority of the 24 species for both dates were not spectrally distinct in any portion of the electromagnetic spectrum. There were nine species in July 2014 and five species in January 2016 that were spectrally distinct in a subset of the measured TIR spectrum. These were not the same species for each date due to seasonality differences in emissivity. For example, TITI was spectrally distinct compared to other species from 10 to 11  $\mu\text{m}$  in July 2014 while in January 2016 most of that spectrally separability was lost.

The random forest classification of species using canopy emissivities confirms results using the SAM and MWU analysis. Species were easily confused among each other with most species having user and producer accuracies  $< 50\%$  (Table 3; Table 4). Overall classification accuracy for July 2014 and January 2016 HyTES imagery was  $< 40\%$  showing that classification of these species using hyperspectral TIR imagery has low performance. Among the highest confused species were LAIN and QUAG with user and producer accuracies  $< 40\%$ . These results demonstrate that species are not spectrally separable in canopy emissivity signatures across both dates.

### 3.3. Canopy LST

Canopy LST distributions for species in July 2014 and January 2016 HyTES imagery were very different (Fig. 7). As expected, due to warmer air conditions, July 2014 had a higher range of observed LSTs compared to January 2016. When comparing species distributions between the two dates, 20 out of 24 species had significantly different distributions. Comparing species pairs, LST distributions also revealed significant differences between dates using ANOVA (Fig. 8). In 2014, 48

more species pairs were significantly different compared to 2016 data. In 2014, five species (ALAR, FICO, FITH, MELI, PEAF) were very distinct from the other nineteen species. In contrast, 2016 had only two species (CHSP and SABA) that were very distinct from the other species. Species with similar canopy architecture did not have significantly different LST distributions, such as two bamboo species (BABE and BATU) with uniform canopies and the two Ficus species (FICO and FITH) with closed dense canopies.

Variables derived from the LiDAR dataset were found to correlate strongly with LST distributions in 2014 and 2016 (Fig. 9; Table S1; Table S2). A tree's neighbors within a 5 m radius were strongly correlated with the tree's canopy LST. Specifically, the presence of pavement in the neighborhood resulted in higher canopy LSTs because of the sensible heat release from dark asphalt pavements. However, if the tree was surrounded by other trees, the canopy LST was lower, presumably due to the increase of latent heat flux. In July 2014, increased presence of grass/shrub, bare soil, and roads as neighbors were correlated with higher canopy LSTs. However, this correlation was not present in January 2016, which was flown in cooler ambient LSTs. Tree height was found to be significantly negatively correlated with 2014 and 2016 LSTs. As the only shrub in this study, ALAR's LSTs were measured from multiple individuals that formed a large aloe patch on the side of a hill. Due to the architecture and height of these plants, ALAR had the highest LST for July 2014 compared to other species. Meanwhile FICO, the tallest species in this study, experienced LST values that did not vary much from air temperatures on either date.

Canopy density, as measured by the number of LiDAR returns, was also found to impact canopy LSTs, but more so in warm ambient air conditions. Dense, closed canopies (e.g. FICO, BABE, and BATU) had cooler LSTs and a smaller range of LST, even on the hot 2014 July day. Low density canopies had a larger substrate influence and experienced higher LSTs, especially if the substrate was man-made and ambient conditions were warm. Species with open tree canopies had warmer LSTs and experienced a larger range of LSTs, mainly caused by the influence of the substrate below the canopy. For example, in January CHSP and CHIN species had dropped their leaves for the season, thus exposing the substrate beneath. In July, CHSP and CHIN had a closed canopy, and LST distributions were not significantly different from most species.

**Table 3**  
Confusion matrix for random forest classification of plant species using the July 2014 HyTES imagery.

	ALAR	BABE	BATU	BRDI	BRRU	CACA	CALE	CEDE	CHIN	CHSP	FICO	FTIH	LAIN	MAGR	MELI	PEAF	POGR	QUAG	QUIL	QURO	QUSU	QUVI	SABA	TITI
ALAR	<b>96</b>	3	4	2	6	5	23	0	3	0	5	10	0	3	1	3	7	0	3	0	6	0	0	
BABE	3	<b>115</b>	9	5	4	2	1	3	6	14	0	5	3	4	2	17	5	2	15	1	6	1	6	
BATU	2	20	<b>197</b>	22	10	2	5	35	11	8	16	27	7	7	11	35	22	33	17	3	1	5	9	
BRDI	10	10	8	<b>186</b>	30	7	15	21	18	15	2	14	19	18	22	5	21	19	3	19	7	23	1	
BRRU	10	13	2	21	<b>123</b>	1	6	10	4	3	2	9	18	6	2	14	30	30	8	3	3	10	5	
CACA	14	4	5	3	1	<b>86</b>	4	2	7	3	2	0	12	1	0	1	4	5	1	2	1	0	3	
CALE	22	2	13	10	15	3	<b>153</b>	4	2	9	9	17	7	5	5	17	24	10	4	6	13	1	6	
CEDE	13	16	14	7	4	10	<b>168</b>	24	13	6	10	15	10	13	29	15	4	9	23	24	21	19		
CHIN	7	12	11	13	11	1	2	7	<b>123</b>	4	13	19	30	7	8	10	12	14	1	12	2	9	8	
CHSP	13	15	7	28	14	8	11	17	8	<b>134</b>	2	6	22	24	6	13	11	21	15	7	5	15	22	
FICO	0	0	8	5	0	4	17	10	15	2	<b>139</b>	31	10	5	28	0	17	22	1	0	5	6	25	
FTIH	0	1	21	12	5	9	12	22	13	2	40	<b>213</b>	10	2	29	16	16	4	1	20	9	9	1	
LAIN	22	16	21	24	10	17	8	19	20	7	3	<b>146</b>	11	23	7	28	23	8	3	2	6	10	6	
MAGR	0	2	2	9	4	0	4	8	2	16	2	<b>137</b>	3	20	0	7	8	28	6	8	9	8	13	
MELI	2	0	3	22	5	0	19	6	5	7	6	<b>21</b>	15	4	<b>167</b>	1	15	21	7	3	9	2	7	
PEAF	3	7	6	17	5	3	9	13	5	11	0	7	6	6	0	<b>127</b>	5	6	13	6	3	4	15	
POGR	7	18	7	21	20	8	18	30	26	25	10	24	27	10	19	5	<b>201</b>	27	4	14	8	12	21	
QUAG	16	39	36	48	17	5	25	20	15	18	28	13	35	26	20	29	<b>216</b>	29	23	17	19	26	33	
QUIL	4	17	9	7	9	12	10	9	21	0	3	6	13	6	10	8	<b>98</b>	6	1	1	3	18		
QURO	6	10	1	6	3	7	4	10	17	5	0	3	11	3	8	9	10	9	3	<b>98</b>	1	9	7	
QUSU	1	4	1	3	6	1	9	9	0	3	0	3	1	6	1	4	5	5	2	0	<b>97</b>	2	8	
QUVI	6	16	7	16	13	7	11	7	13	4	7	12	19	10	8	19	20	5	5	12	<b>158</b>	26	18	
SABA	0	2	11	3	2	3	5	17	7	38	12	15	11	22	13	4	22	13	8	5	13	21	11	
TITI	5	11	14	7	18	15	8	13	4	20	0	0	11	38	1	18	3	31	36	11	3	23	14	
User	52.5	41.8	38.6	36.9	36.6	52.1	42.6	35.4	36.6	30.5	39.7	44.1	33.0	45.1	48.1	45.2	35.4	28.0	32.6	38.1	56.1	37.1	45.0	
Producer	38.4	32.9	49.3	37.2	35.1	43.0	38.3	37.3	35.1	33.5	46.3	47.3	32.4	34.3	41.8	36.3	33.2	32.7	39.2	38.8	39.5	46.9	47.8	
Overall	38.7																							
Kappa	0.36																							

Bold on the diagonal designates the number of pixels correctly classified.

**Table 4**  
Confusion matrix for random forest classification of plant species using the January 2016 HyTES imagery.

	ALAR	BABE	BATU	BRDI	BRRU	CACA	CALE	CEDE	CHIN	CHSP	FICO	FTTH	LAIN	MAGR	MELI	PEAF	POGR	QUAG	QUIL	QURO	QUSU	QUVI	SABA	TITI
ALAR	<b>102</b>	3	0	4	6	3	5	1	15	0	2	11	8	2	6	4	0	3	0	0	8	14	1	1
BABE	1	<b>171</b>	14	4	5	6	4	3	9	10	2	19	7	4	4	16	24	13	16	9	1	11	13	13
BRDU	0	32	<b>177</b>	27	13	1	3	34	6	0	14	12	9	15	13	5	13	33	12	13	6	8	15	16
BRRU	16	34	40	<b>238</b>	39	9	11	44	12	8	13	25	30	7	22	28	32	33	12	24	5	12	7	34
CACA	0	11	21	53	<b>230</b>	0	10	7	10	1	37	18	32	5	15	1	16	29	1	21	6	24	20	7
CALE	7	8	0	6	7	<b>125</b>	3	6	5	3	3	0	13	9	2	5	4	6	11	2	0	19	8	9
CEDE	15	26	2	25	26	2	<b>215</b>	8	14	18	14	7	23	0	8	10	8	13	16	6	8	16	6	12
CHIN	1	8	25	20	18	7	3	<b>187</b>	0	3	17	19	12	30	22	1	32	12	12	1	21	10	8	8
CHSP	6	7	7	12	3	3	13	0	<b>123</b>	12	5	5	9	3	2	1	1	5	31	7	10	1	14	34
FICO	1	1	13	18	11	4	7	18	0	<b>15</b>	200	15	18	34	5	5	11	10	27	21	3	4	14	24
FTTH	4	17	23	16	13	5	7	25	11	9	16	217	8	19	13	2	36	17	12	11	9	18	9	9
LAIN	5	18	0	26	23	12	13	7	9	21	8	5	<b>188</b>	14	16	8	34	17	5	5	6	12	25	23
MAGR	24	0	18	9	6	15	2	26	11	20	11	10	<b>167</b>	13	6	42	13	12	5	18	1	21	21	21
MELI	4	4	11	9	18	1	0	19	5	5	7	8	<b>162</b>	2	15	22	0	6	3	13	12	5	12	5
PEAF	12	15	0	11	1	10	22	3	9	8	0	17	24	6	1	<b>127</b>	1	6	6	6	0	20	10	10
POGR	3	22	15	22	24	13	9	45	1	27	32	47	20	52	20	15	<b>266</b>	45	24	9	15	8	23	18
QUAG	0	30	39	32	26	10	6	46	27	22	18	37	17	29	35	23	<b>49</b>	33	19	33	23	5	32	36
QUIL	17	11	1	0	33	17	9	27	12	0	14	5	1	3	15	6	<b>18</b>	145	7	6	11	10	7	7
QURO	0	6	5	1	12	0	1	7	3	4	4	3	12	2	13	4	7	8	7	7	2	122	2	20
QUSU	0	3	8	7	4	1	8	0	2	7	1	0	11	4	3	1	11	9	7	2	103	0	8	24
QUVI	8	8	7	10	28	14	19	26	20	14	3	22	8	6	2	10	24	6	9	3	<b>216</b>	27	9	9
SABA	2	4	8	10	7	6	2	13	23	8	2	9	20	6	7	15	15	17	18	9	1	21	190	11
TITI	2	8	14	32	20	4	13	4	14	8	5	12	16	33	7	14	10	28	17	9	14	6	10	231
User	50.7	44.9	37.1	32.4	40.0	47.9	43.2	39.3	35.8	40.8	39.0	40.1	40.6	33.3	47.4	37.3	34.3	37.7	34.9	51.0	46.0	41.5	44.8	43.5
Producer	40.8	38.0	39.3	39.7	41.8	41.7	53.8	34.0	35.1	44.4	43.3	39.5	34.2	37.1	40.5	36.3	40.9	44.1	36.3	34.9	41.1	43.2	34.5	42.0
Overall	39.9																							
Kappa	0.37																							

Bold on the diagonal designates the number of pixels correctly classified.

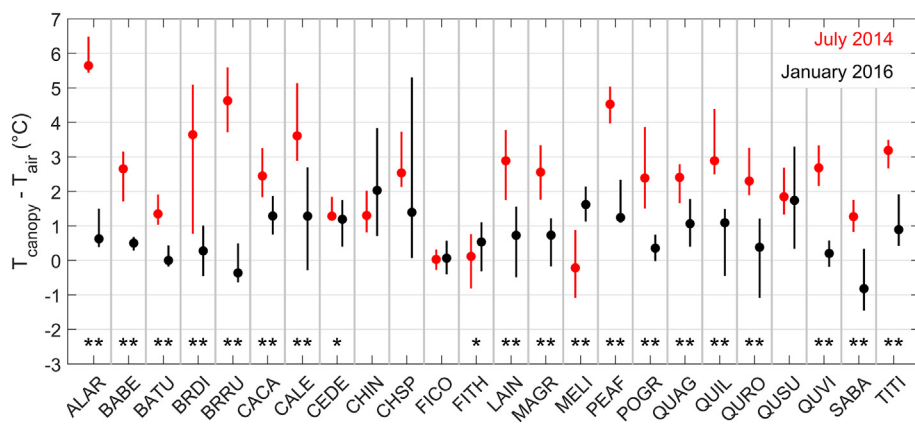


Fig. 7. 2014 and 2016 canopy LST distributions (canopy LST minus air temperature) for each species. Circles are median LSTs with the top and bottom of bars marking the 25th and 75th quartiles. Asterisks designate significant differences between 2014 and 2016 LST distributions (\* p < 0.05, \*\* p < 0.01).

## 4. Discussion

### 4.1. Plant species' leaf emissivity variability

In this study, we quantified the spectral separability of plant species' leaf level emissivities. We found that leaf emissivities were unique for approximately one third of the 24 plant species analyzed in this study. This remained true even when leaf emissivities were resampled from over 177 wavelengths to HyTES' 155 wavelengths between 8 and 11  $\mu\text{m}$ . Thirty out of 276 species pairs were separable based on spectral shape, while 91 species pairs were separable based on the total number of wavelengths that were significantly different. Our results show that some plant species exhibit unique spectral features at the leaf level that distinguish them spectrally. However, not all species in this study were spectrally unique. In contrast, other researchers have found that most of the species they studied are spectrally separable. Using 13 common garden species in the Netherlands, Ullah et al. (2012a) found that 76 out of 78 species pairs had significantly different Jefferies Matusita distances. In a direct comparison to the previous study, Rock et al. (2016) classified eight species with 92% overall accuracy but stipulated that high signal-to-noise ratio was necessary. Another study successfully classified 19 species with a kappa of 0.94 (Buitrago et al., 2018). However, there are a few studies that also found confusion between

species. In a study mirroring results similar to ours, Harrison et al. (2018) classified 26 tropical species and found most species were spectrally similar with the exception of five. Lastly, a study classified 32 species at the canopy with an overall accuracy of only 83% and also found that leaf emissivities contained more spectral separability than the canopy (Ribeiro da Luz, 2006).

When discussing the separability of plant species in the TIR, it is common to identify wavelengths that contain the most discriminating power. The largest discriminating power among species was found in the 2.5–8  $\mu\text{m}$  wavelengths, which have been identified as containing key information for species discrimination or leaf trait retrieval (Buitrago Acevedo et al., 2017; Buitrago et al., 2018, 2016; Meerink et al., 2016). However, HyTES does not measure between 2.5 and 7.5  $\mu\text{m}$  because this region is complicated due to the long wavelength edge of the solar radiation curve, strong water vapor absorption, and the short wavelength edge of the terrestrial emittance curve (Gates et al., 1965). The range of emissivities retrieved from HyTES in the atmospheric window region (8–11  $\mu\text{m}$ ) did not contain as much spectral discrimination for species in our study. As in other studies, plant species tend to be featureless in this region with weaker absorption features (Elvidge, 1988). In the HyTES measured TIR spectrum, our study identified key wavelengths at 8.5, 10.04  $\mu\text{m}$ , which are related to known features of water absorption and cellulose (Elvidge, 1988).

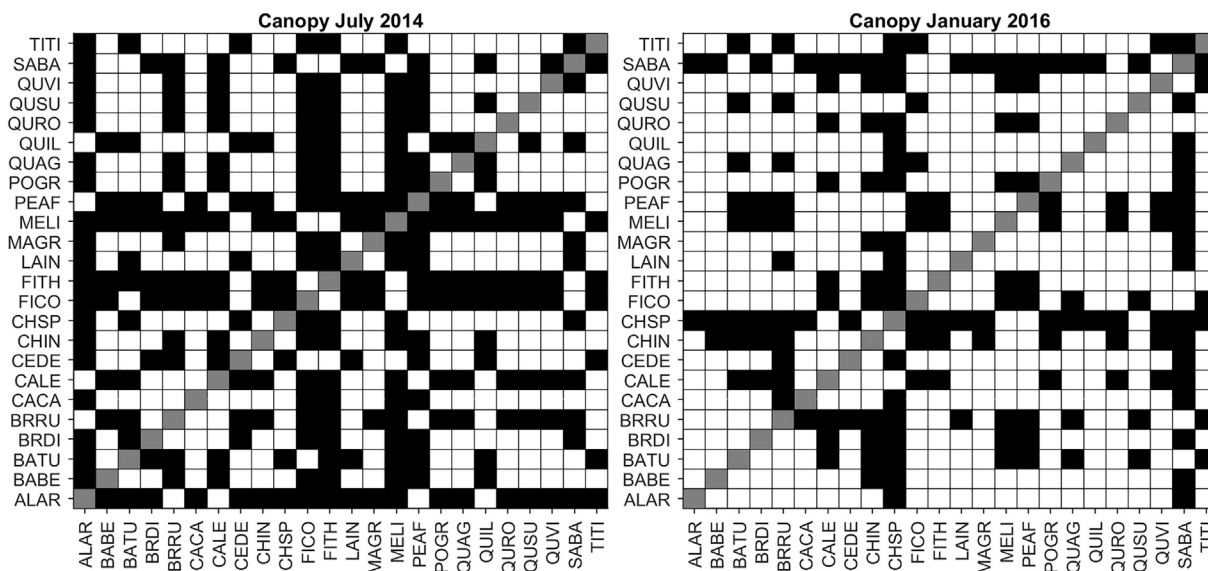
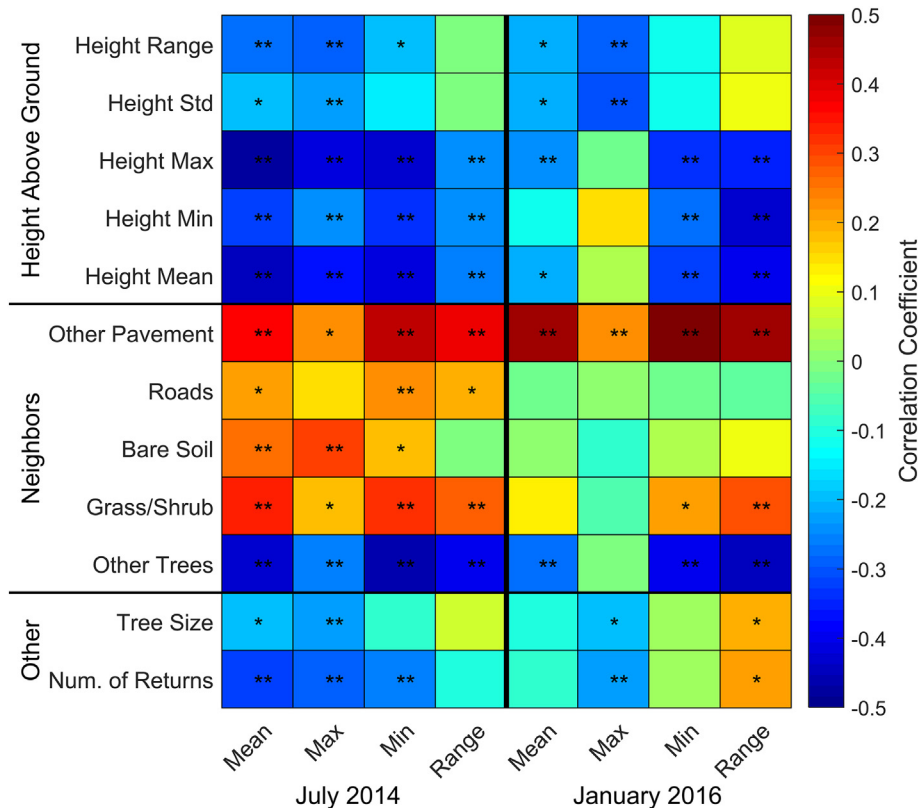


Fig. 8. LST comparison between species pairs for 2014 (left) and 2016 (right) imagery. Black squares designate significant differences between species LST distributions (p < 0.05).



**Fig. 9.** Correlations between 2014 and 2016 LST statistics (x-axis) and LiDAR derived variables (y-axis). Asterisks designate significant differences in correlations (\*  $p < 0.05$ , \*\*  $p < 0.01$ ). Correlations between all variables and 2014 and 2016 LST are available in Tables S1 and S2.

While we did not relate leaf emissivities to leaf traits, other studies suggest that leaf traits expressed in the TIR promote species identification at the leaf level and potentially at the canopy (Ribeiro da Luz and Crowley, 2010).

#### 4.2. Plant species' canopy emissivity variability

We found, for the same set of species, that canopy emissivity for July 2014 and January 2016 HyTES imagery does not contain the magnitude of separability among species as seen at the leaf level. No species showed clear separability based on spectral shape, and only 29 and 54 out of 276 species pairs had  $> 80\%$  of wavelengths significantly different for July 2014 and January 2016, respectively. When determining influential wavelengths for species discrimination, ten out of 24 species had regions of the TIR that were significantly different. Species had more variability within species than between species, which easily confused species discrimination. Although images were collected in different seasons and years, the canopy emissivities showed limited variation for evergreen species.

Very few studies have examined canopy spectral emissivity, mainly due to the lack of data at desired spectral and spatial resolutions. In controlled laboratory settings, canopy emissivities have been found to be significantly different for four species, and increases in LAI correspond to increases in emissivity (Neinavaz et al., 2016). Also in laboratory settings, stress studies have found that increasing water stress causes emissivity to increase due to blackbody cavity effects (Buitrago et al., 2016; Gerhards et al., 2016). While these studies demonstrate opportunities for canopy emissivity, they have been restricted to fine spatial resolution imagery collected in controlled settings. Only one study, to our knowledge, has examined canopy emissivity characteristics collected using airborne imagery. Ribeiro Da Luz and Crowley (2010) successfully classified approximately 25 species using 1 m spatial resolution imagery from the SEBASS sensor. However, this was only

half of the species studied, with the remainder not being spectrally separable.

#### 4.3. Land surface temperature (LST) pattern among species

Finally, temperature patterns across species were significantly different between the July 2014 and January 2016 HyTES imagery, corresponding to ambient air temperatures that were 31 °C and 22 °C, respectively. In the warmer ambient air conditions experienced in July 2014 imagery, species' LST distributions were found to be significantly different in 129 out of 276 species pairs. In cooler ambient air conditions, only 81 species pairs were significantly different. Other studies have also found species-specific differences in LST distributions. For example, Leuzinger et al. (2010) found that trees with small leaves were cooler than large leaf trees while Meier and Scherer (2012) showed that deciduous trees had higher LST variation in the canopy compared to conifers. Urban tree canopy LSTs depend on species-specific properties and the location of the tree (Leuzinger and Körner, 2007; Meier and Scherer, 2012).

We found that LST distributions were highly correlated with a tree's neighboring pixel land cover type. Other trees and pavement as neighbors had the highest influence on canopy LSTs. This corresponds to a study that found that substrate can impact the tree temperature where grass is cooler than a sealed surface like asphalt or concrete (Kjelgren and Montague, 1998; Leuzinger et al., 2010; Montague and Kjelgren, 2004). In our study, the added complexity of a tree's architecture and tree height were negatively correlated with LST. In our study site and a mixed deciduous forest in NW Switzerland, open canopies exhibited mean canopy leaf temperatures close to air temperature, and dense canopies exhibited warmer than air temperatures (Leuzinger and Körner, 2007).

#### 4.4. Considerations

This study explored the application of HyTES imagery for plant species' emissivity and LST research. Our findings expose the limitations to be considered for future research. In this study, leaf samples were not collected at the same time as the imagery, so differences between leaf and canopy might be related to phenology differences. The stability of leaf emissivities over the season and years has not been studied, so it cannot be said how influential phenology is on emissivity. Additionally, we had a small sample size for leaf measurements due to time constraints and the number of individuals available in the Huntington Gardens. A more comprehensive and systematic sampling is required to fully study the scaling of leaf emissivities to canopies, including the measurement of tree characteristics such as leaf area index. In the TIR domain, scaling is complicated due to several factors that weaken already subtle plant features including canopy voids, leaf angle, canopy structure, and errors in temperature emissivity separation (Ribeiro Da Luz and Crowley, 2010, 2007; Salisbury, 1986). Ribeiro Da Luz and Crowley (2007) confirmed the complication of scaling when taking measurements from a field of view of 6.4 cm to 44 cm and experiencing progressive attenuation of the spectral emissivity features. Ribeiro Da Luz and Crowley (2010) found that canopy geometry and composition including leaf morphology, leaf disposition (e.g. planophile or erectophile), canopy closure, and size of canopy were the largest controlling factors. Radiative transfer models could be used to account for the scattering and absorption of radiation inside canopies when scaling (Francois et al., 1997; Jacob et al., 2017; Olioso, 1995; Snyder and Wan, 1998; Verhoef et al., 2007). These models incorporate additional variables including directional gap fraction, angular cavity effect coefficients, and better incorporation of soil contribution. Without the use of radiative transfer models, relationships developed using leaf emissivities will not be directly translatable to the canopy for future airborne or spaceborne missions.

In addition to improved sampling techniques, future projects should be mindful of the HyTES sensor development and sensor specifications. The signal-to-noise ratio (SNR) of the HyTES sensor might have reduced separation ability especially since many of the differences between species' temperature and emissivities were small in magnitude. In this study, we restricted our analysis to 8.3–11 μm where the mean Noise Equivalent delta Temperature (NEDT) is 0.17 °C because the SNR increases significantly outside of this spectral range (Meerdink et al., 2016). However, the lower SNR would decrease the separability of species emissivities and ultimately temperatures. Lastly, errors may be present in canopy emissivity and LST products. These products are calculated through an iterative Temperature Emissivity Separation (TES) algorithm developed by NASA JPL, which has been adapted to 256 HyTES radiance bands. However, due to the relatively new deployment of this sensor, the algorithm is undergoing refinement to improve atmospheric correction accuracy, especially as new applications are presented that require emissivity retrievals with high accuracy.

While our study found that species classification using TIR is difficult at the canopy level, this study does present opportunities for a mission recently deployed. In June 2018, the ECOSTRESS sensor was launched with the primary goal of measuring plant temperatures in order to understand how much water plants need and how they respond to stress. The sensor was installed on the International Space Station and provides data with a 38-m in-track by 69-m cross-track spatial resolution, five spectral bands in the 8–12.5 μm range, and a predicted temperature sensitivity of ≤0.15 K at 300 K (<https://ecostress.jpl.nasa.gov/instrument>). This study directly supports future ECOSTRESS research questions for vegetation emissivity and LST. For example, the ECOSTRESS mission will be delivering an evapotranspiration product for the continental USA and over key biomes around the world. A key assumption of the evapotranspiration models requires that vegetation emissivity does not vary by species. This analysis gives insight into the

amount of error introduced into models that calculate evapotranspiration.

#### 5. Conclusions

The development of NASA's HyTES hyperspectral thermal sensor has opened up the possibility of using high spectral resolution emissivity and fine spatial resolution LST for vegetation research. In this study we set out to answer three questions. First, we asked if plant species were spectrally separable using leaf level emissivities. We found that 20 out of 24 plant species were spectrally separable through spectral shape or the number of wavelengths containing significantly different emissivities. Second, we asked if this species variability extended to canopy emissivities collected from July 2014 and January 2016 HyTES imagery. We found that plant species lost most of the spectral separability observed at the leaf level when scaled to canopy emissivities. Finally, we asked what LST patterns are exhibited by plant species across dates and how does the variability relate to canopy attributes. We found that species' canopy LSTs displayed unique distributions across dates and among species. Many of these distributions could be explained by canopy geometry, with tree density and height playing key roles. Additionally, species canopy temperatures were highly influenced by a tree's surrounding environment, with neighboring trees creating cooler LST and pavement creating warmer LST conditions.

Our study fills in knowledge gaps in the TIR domain for both emissivity and LST. Previously, only one study has examined plant species using high spectral resolution airborne TIR imagery. Our results demonstrate that only a few spectrally distinct species in the Huntington Gardens were separable at the canopy level and that leaf level relationships derived empirically in the laboratory will not directly translate to the canopy. Most of the unique spectral characteristics measured in laboratory conditions are not retained at the canopy due to multiple scattering which involves emission, reflection, and absorption. However, the HyTES fine spatial resolution LST imagery has provided a deeper understanding of LST variability across plant species which exhibit different canopy attributes. LST is primarily used to measure plant stress, but we found that plant species still exhibit variability in temperature distributions even in ideal water conditions.

With the launch of the ECOSTRESS mission and continued image collection of HyTES, more TIR imagery will become available to the scientific community. This study begins to explore the application of such a dataset for the purposes of vegetation research, specifically how much variability there is among plant species. As research expands in the TIR domain, our understanding of plants' variability in TIR spectral signatures and LST will become increasingly important. Advancing this research for vegetation canopies may enable new types of remote sensing observations that are distinct from other portions of the electromagnetic spectrum.

#### Acknowledgments

We thank the Huntington Gardens, specifically Sean Lahmeyer and David Sivertsen, for their support in collecting leaf samples and sharing data. We thank Elsa Abbott and Bill Johnson for their assistance measuring leaf emissivities at NASA JPL. We would like to acknowledge Sari Blakeley, Rafael Ramos, and Kelly Caylor for their comments throughout the development of this manuscript. This project was funded as a NASA JPL Subcontract titled "Plant species mapping, water, and LMA using HyTES" and a NASA Earth and Space Science Fellowship (NESSF). Jan Pisek and Kairi Adamson were supported by the Estonian Research Council grant PUT1355 and Mobilitas Pluss MOBERC-11.

#### Appendix A. Supplementary data

Supplementary data to this article can be found online at <https://doi.org/10.1016/j.rse.2019.02.018>.

[doi.org/10.1016/j.rse.2019.02.009](https://doi.org/10.1016/j.rse.2019.02.009).

## References

- Anderson, M., Kustas, W., 2008. Thermal remote sensing of drought and evapotranspiration. *Eos* 89, 233–234. <https://doi.org/10.1029/2008EO260001>.
- Anderson, M.C., Norman, J.M., Kustas, W.P., Houborg, R., Starks, P.J., Agam, N., 2008. A thermal-based remote sensing technique for routine mapping of land-surface carbon, water and energy fluxes from field to regional scales. *Remote Sens. Environ.* 112, 4227–4241. <https://doi.org/10.1016/j.rse.2008.07.009>.
- Anderson, M.C., Zolin, C.A., Sentelhas, P.C., Hain, C.R., Semmens, K., Yilmaz, M.T., Gao, F., Otkin, J.A., Tetrault, R., 2016. The evaporative stress index as an indicator of agricultural drought in Brazil: an assessment based on crop yield impacts. *Remote Sens. Environ.* 174, 82–99. <https://doi.org/10.1016/j.rse.2015.11.034>.
- Arshad, M., Ali, A., 2018. Estimation of leaf water content from mid- and thermal-infrared spectra by coupling genetic algorithm and partial least squares regression. *J. Appl. Remote. Sens.* 12. <https://doi.org/10.1111/jrse.122203>.
- Belgiu, M., Dragut, L., 2016. Random forest in remote sensing: a review of applications and future directions. *ISPRS J. Photogramm. Remote Sens.* 114, 24–31. <https://doi.org/10.1016/j.isprsjprs.2016.01.011>.
- Borel, C., 2008. Error analysis for a temperature and emissivity retrieval algorithm for hyperspectral imaging data. *Int. J. Remote Sens.* 29, 5029–5045. <https://doi.org/10.1080/01431160802036540>.
- Buitrago Acevedo, M.F., Groen, T.A., Hecker, C.A., Skidmore, A.K., 2017. Identifying leaf traits that signal stress in TIR spectra. *ISPRS J. Photogramm. Remote Sens.* 125, 132–145. <https://doi.org/10.1016/j.isprsjprs.2017.01.014>.
- Buitrago, M.F., Groen, T.A., Hecker, C.A., Skidmore, A.K., 2016. Changes in thermal infrared spectra of plants caused by temperature and water stress. *ISPRS J. Photogramm. Remote Sens.* 111, 22–31. <https://doi.org/10.1016/j.isprsjprs.2015.11.003>.
- Buitrago, M.F., Skidmore, A.K., Groen, T.A., Hecker, C.A., 2018. Connecting infrared spectra with plant traits to identify species. *ISPRS J. Photogramm. Remote Sens.* 139, 183–200. <https://doi.org/10.1016/j.isprsjprs.2018.03.013>.
- Calderón, R., Navas-Cortés, J.A., Lucena, C., Zarco-Tejada, P.J., 2013. High-resolution airborne hyperspectral and thermal imagery for early detection of Verticillium wilt of olive using fluorescence, temperature and narrow-band spectral indices. *Remote Sens. Environ.* 139, 231–245. <https://doi.org/10.1016/j.rse.2013.07.031>.
- Cheng, J., Liang, S., Wang, J., Li, X., 2010. A stepwise refining algorithm of temperature and emissivity separation for hyperspectral thermal infrared data. *IEEE Trans. Geosci. Remote Sens.* 48, 1588–1597. <https://doi.org/10.1109/TGRS.2009.2029852>.
- Curran, P.J., 1989. Remote sensing of foliar chemistry. *Remote Sens. Environ.* 30, 271–278. [https://doi.org/10.1016/0034-4257\(89\)90069-2](https://doi.org/10.1016/0034-4257(89)90069-2).
- Elvidge, C.D., 1988. Thermal infrared reflectance of dry plant materials: 2.5–20.0. *Remote Sens. Environ.* 26, 265–285.
- Fabre, S., Lesaignoux, A., Olioso, A., Briottet, X., 2011. Influence of water content on spectral reflectance of leaves in the 3–15 μm domain. *IEEE Geosci. Remote Sens. Lett.* 8, 143–147.
- Fisher, J.B., Tu, K.P., Baldocchi, D.D., 2008. Global estimates of the land-atmosphere water flux based on monthly AVHRR and ISLSCP-II data, validated at 16 FLUXNET sites. *Remote Sens. Environ.* 112, 901–919. <https://doi.org/10.1016/j.rse.2007.06.025>.
- Francois, C., Ottle, C., Prevot, L., 1997. Analytical parameterization of canopy directional emissivity and directional radiance in the thermal infrared. Application on the retrieval of soil and foliage temperatures using two directional measurements. *Int. J. Remote Sens.* 18, 2587–2621. <https://doi.org/10.1080/014311697217495>.
- Fuchs, M., 1990. Infrared measurement of canopy temperature and detection of plant water stress. *Theor. Appl. Climatol.* 42, 253–261.
- Fuchs, M., Tanner, C.B., 1966. Infrared thermometry of vegetation. *Agron. J.* 58, 597–601.
- Gates, D.M., Tantraporn, W., 1952. The reflectivity of deciduous trees and herbaceous plants in the infrared to 25 microns. *Science* 115, 613–616 80.
- Gates, D.M., Keegan, H.J., Schleter, J.C., Weidner, V.R., 1965. Spectral properties of plants. *Appl. Opt.* 4, 11–20. <https://doi.org/10.1364/AO.4.000011>.
- Gerhards, M., Rock, G., Schlerf, M., Udelhoven, T., 2016. Water stress detection in potato plants using leaf temperature, emissivity, and reflectance. *Int. J. Appl. Earth Obs. Geoinf.* 53, 27–39. <https://doi.org/10.1016/j.jag.2016.08.004>.
- Gillespie, A., Rokugawa, S., Matsunaga, T., Steven Cothorn, J., Hook, S., Kahle, A.B., 1998. A temperature and emissivity separation algorithm for advanced spaceborne thermal emission and reflection radiometer (ASTER) images. *IEEE Trans. Geosci. Remote Sens.* 36, 1113–1126. <https://doi.org/10.1109/36.700995>.
- Grant, O.M., Tronina, L., Jones, H.G., Chaves, M.M., 2007. Exploring thermal imaging variables for the detection of stress responses in grapevine under different irrigation regimes. *J. Exp. Bot.* 58, 815–825. <https://doi.org/10.1093/jxb/erl153>.
- Hackwell, J.A., Warren, D.W., Bongiovanni, R.P., Hansel, S.J., Hayhurst, T.L., Hackwell, J.A., Warren, D.W., Bongiovanni, R.P., Hansel, S.J., Hayhurst, T.L., Mabry, D.J., Sivjee, M.G., Skinner, J.W., 1996. LWIR/MWIR imaging hyperspectral sensor for airborne and ground-based remote sensing. In: Proc. SPIE 2819, Imaging Spectrom. II. 2819. pp. 102–107. <https://doi.org/10.1117/12.258057>.
- Harrison, D., Rivard, B., Sánchez-Azofeifa, A., 2018. Classification of tree species based on longwave hyperspectral data from leaves, a case study for a tropical dry forest. *Int. J. Appl. Earth Obs. Geoinf.* 66, 93–105. <https://doi.org/10.1016/j.jag.2017.11.009>.
- Hook, S.J., Johnson, W.R., Abrams, M.J., 2013. NASA's hyperspectral thermal emission spectrometer (HyTES). In: Kuenzer, C., Dech, S. (Eds.), *Thermal Infrared Remote Sensing: Sensors, Methods, Applications, Remote Sensing and Digital Image Processing*. Springer, Dordrecht, pp. 93–115. <https://doi.org/10.1007/978-94-007-6639-6>.
- Hook, S.J., Hulley, G.C., Johnson, W.R., Eng, B., Mihaly, J., Chazanoff, S., Vance, N., Staniszewski, Z., Rivera, G., Holmes, K.T., Guillevic, P., 2019. The hyperspectral thermal emission spectrometer (HyTES) – a new hyperspectral thermal infrared airborne imager for earth science. *Remote Sens. Environ.* (in press).
- Hulley, G.C., Hook, S.J., 2011. HySPR1 level-2 thermal infrared (TIR) land surface temperature and emissivity algorithm theoretical basis document. In: *NASA Technical Reports*.
- Hulley, G.C., Duren, R.M., Hopkins, F.M., Hook, S.J., Vance, N., Guillevic, P., Johnson, W.R., Eng, B.T., Mihaly, J.M., Jovanovic, V.M., Chazanoff, S.L., Staniszewski, Z.K., Kuai, L., Worden, J., Frankenberg, C., Rivera, G., Aubrey, A.D., Miller, C.E., Malakar, N.K., Sánchez Tomás, J.M., Holmes, K.T., 2016. High spatial resolution imaging of methane and other trace gases with the airborne hyperspectral thermal emission spectrometer (HyTES). *Atmos. Meas. Tech. Discuss.* 1–32. <https://doi.org/10.5194/amt-2016-8>.
- Iqbal, A., Ullah, S., Khalid, N., Ahmad, W., Ahmad, I., Sha, M., Hulley, G.C., Roberts, D.A., Skidmore, A.K., 2018. Selection of HySPR1 optimal band positions for the earth compositional mapping using HyTES data. *Remote Sens. Environ.* 206, 350–362. <https://doi.org/10.1016/j.rse.2017.12.005>.
- Islam, T., Hulley, G.C., Malakar, N.K., Radocinski, R.G., Guillevic, P.C., Hook, S.J., 2017. A physics-based algorithm for the simultaneous retrieval of land surface temperature and emissivity from VIIRS thermal infrared data. *IEEE Trans. Geosci. Remote Sens.* 55, 563–576. <https://doi.org/10.1109/TGRS.2016.2611566>.
- Jackson, R.D., Reginato, R.J., Idso, S.B., 1977. Wheat canopy temperature: a practical tool for evaluating water requirements. *Water Resour. Res.* 13, 651–656.
- Jackson, R.D., Idso, S.B., Reginato, R.J., Pinter Jr., P.J., 1981. Canopy temperature as a crop water stress indicator. *Water Resour. Res.* 17, 1133–1138.
- Jackson, R.D., Kustas, W.P., Choudhury, B.J., 1988. A reexamination of the crop water stress index. *Irrig. Sci.* 9, 309–317. <https://doi.org/10.1007/BF00296705>.
- Jacob, F., Lesaignoux, A., Olioso, A., Weiss, M., Caillaud, K., Jacquemoud, S., Nerry, F., French, A., Schmugge, T., Briottet, X., Lagouarde, J.P., 2017. Reassessment of the temperature-emissivity separation from multispectral thermal infrared data: introducing the impact of vegetation canopy by simulating the cavity effect with the SAIL-Thermique model. *Remote Sens. Environ.* 198, 160–172. <https://doi.org/10.1016/j.rse.2017.06.006>.
- Johnson, W.R., Hulley, G., Hook, S.J., 2014. Remote gas plume sensing and imaging with NASA's hyperspectral thermal emission spectrometer (HyTES). In: Proc. SPIE 9101, Next-Generation Spectroscopic Technologies VII, <https://doi.org/10.1117/12.2049005>.
- Jones, H.G., 1999. Use of infrared thermometry for estimation of stomatal conductance as a possible aid to irrigation scheduling. *Agric. For. Meteorol.* 95, 139–149. [https://doi.org/10.1016/S0168-1923\(99\)00030-1](https://doi.org/10.1016/S0168-1923(99)00030-1).
- Jones, H.G., 2014. *Plants and Microclimate: A Quantitative Approach to Environmental Plant Physiology*, Third ed. Cambridge University Press.
- Jones, H.G., Leinonen, I., 2003. Thermal imaging for the study of plant water relations. *J. Agric. Meteorol.* 59, 205–217.
- Jones, H.G., Schofield, P., 2008. Thermal and other remote sensing of plant stress. *Gen. Appl. Plant Physiol.* 34, 19–32 ([doi:10.1.1.399.2918](https://doi.org/10.1.1.399.2918)).
- Jones, H.G., Stoll, M., Santos, T., de Sousa, C., Chaves, M.M., Grant, O.M., 2002. Use of infrared thermography for monitoring stomatal closure in the field: application to grapevine. *J. Exp. Bot.* 53, 2249–2260. <https://doi.org/10.1093/jxb/erf083>.
- Kealy, P.S., Hook, S.J., 1993. Separating temperature and emissivity in thermal infrared multispectral scanner data: Implications for recovering land surface temperatures. *IEEE Trans. Geosci. Remote Sens.* 31, 1155–1164 ([doi:10.1109/36.289293](https://doi.org/10.1109/36.289293)).
- Kjelgren, R., Montague, T., 1998. Urban tree transpiration over turf and asphalt surfaces. *Atmos. Environ.* 32, 35–41. [https://doi.org/10.1016/S1352-2310\(97\)00177-5](https://doi.org/10.1016/S1352-2310(97)00177-5).
- Kogan, F.N., 1995a. Application of vegetation index and brightness temperature for drought detection. *Adv. Space Res.* 15, 91–100. [https://doi.org/10.1016/0273-1177\(95\)00079-T](https://doi.org/10.1016/0273-1177(95)00079-T).
- Kogan, F.N., 1995b. Droughts of the late 1980s in the United States as derived from NOAA polar-orbiting satellite data. *Bull. Am. Meteorol. Soc.* 76, 655–668. [https://doi.org/10.1175/1520-0477\(1995\)076<0655:DOTLT>2.0.CO;2](https://doi.org/10.1175/1520-0477(1995)076<0655:DOTLT>2.0.CO;2).
- Kruse, F.A., 2015. Comparative analysis of Airborne Visible/Infrared Imaging Spectrometer (AVIRIS), and Hyperspectral Thermal Emission Spectrometer (HyTES) longwave infrared (LWIR) hyperspectral data for geologic mapping. In: Proc. SPIE 9472, Algorithms and Technologies for Multispectral, Hyperspectral, and Ultraspectral Imagery XXI, <https://doi.org/10.1117/12.2176646>.
- Kruse, F.A., Lefkoff, A.B., Boardman, J.W., Heidebrecht, K.B., Shapiro, A.T., Barloon, P.J., Goetz, A.F.H., 1993. The spectral image processing system (SIPS)—interactive visualization and analysis of imaging spectrometer data. *Remote Sens. Environ.* 44, 145–163. [https://doi.org/10.1016/0034-4257\(93\)90013-N](https://doi.org/10.1016/0034-4257(93)90013-N).
- Kuai, L., Worden, J.R., Li, K.F., Hulley, G.C., Hopkins, F.M., Miller, C.E., Hook, S.J., Duren, R.M., Aubrey, A.D., 2016. Characterization of anthropogenic methane plumes with the hyperspectral thermal emission spectrometer (HyTES): a retrieval method and error analysis. *Atmos. Meas. Tech.* 9, 3165–3173. <https://doi.org/10.5194/amt-9-3165-2016>.
- LARICAC Product Guide 2006–07, 2006. <http://egis3.lacounty.gov/dataportal/wp-content/uploads/2012/05/ProductGuideFinal.pdf>.
- Leinonen, I., Grant, O.M., Tagliavia, C.P.P., Chaves, M.M., Jones, H.G., 2006. Estimating stomatal conductance with thermal imagery. *Plant Cell Environ.* 29, 1508–1518. <https://doi.org/10.1111/j.1365-3040.2006.01528.x>.
- Leuzinger, S., Körner, C., 2007. Tree species diversity affects canopy leaf temperatures in a mature temperate forest. *Agric. For. Meteorol.* 146, 29–37. <https://doi.org/10.1016/j.agrformet.2007.05.007>.
- Leuzinger, S., Zotz, G., Asshoff, R., Körner, C., 2005. Responses of deciduous forest trees to severe drought in Central Europe. *Tree Physiol.* 25, 641–650. <https://doi.org/10.1093/treephys/25.5.641>.

- 1093/treephys/25.6.641.
- Leuzinger, S., Vogt, R., Körner, C., 2010. Tree surface temperature in an urban environment. *Agric. For. Meteorol.* 150, 56–62. <https://doi.org/10.1016/j.agrformet.2009.08.006>.
- Liu, W.T., Kogan, F.N., 1996. Monitoring regional drought using the vegetation condition index. *Int. J. Remote Sens.* 17, 2761–2782. <https://doi.org/10.1080/01431169608949106>.
- Malakar, N.K., Hulley, G.C., 2016. A water vapor scaling model for improved land surface temperature and emissivity separation of MODIS thermal infrared data. *Remote Sens. Environ.* 182, 252–264. <https://doi.org/10.1016/j.rse.2016.04.023>.
- Matsunaga, T., 1994. A temperature-emissivity relationship between the mean, the maximum, and the minimum of the thermal infrared emissivity spectrum. *J. Remote Sens. Soc. Jpn.* 14, 28–39. <https://doi.org/10.11440/rssj1981.14.230>.
- Meerdink, S.K., Roberts, D.A., King, J.Y., Roth, K.L., Dennison, P.E., Amaral, C.H., Hook, S.J., 2016. Linking seasonal foliar traits to VSWIR-TIR spectroscopy across California ecosystems. *Remote Sens. Environ.* 186, 322–338. <https://doi.org/10.1016/j.rse.2016.08.003>.
- Meier, F., Scherer, D., 2012. Spatial and temporal variability of urban tree canopy temperature during summer 2010 in Berlin, Germany. *Theor. Appl. Climatol.* 110, 373–384. <https://doi.org/10.1007/s00704-012-0631-0>.
- Montague, T., Kjelgren, R., 2004. Energy balance of six common landscape surfaces and the influence of surface properties on gas exchange of four containerized tree species. *Sci. Hortic.* 100, 229–249. <https://doi.org/10.1016/j.scientia.2003.08.010>.
- Neinavaz, E., Darvishzadeh, R., Skidmore, A.K., Groen, T.A., 2016. Measuring the response of canopy emissivity spectra to leaf area index variation using thermal hyperspectral data. *Int. J. Appl. Earth Obs. Geoinf.* 53, 40–47. <https://doi.org/10.1016/j.jag.2016.08.002>.
- Olioso, A., 1995. Simulating the relationship between thermal emissivity and the normalized difference vegetation index. *Int. J. Remote Sens.* 16, 3211–3216. <https://doi.org/10.1080/01431169508954625>.
- Otkin, J.A., Anderson, M.C., Hain, C.R., Mladenova, I.E., Basara, J.B., Svoboda, M., 2013. Examining rapid onset drought development using the thermal infrared-based evaporative stress index. *Am. Meteorol. Soc.* 14, 1057–1074. <https://doi.org/10.1175/JHM-D-12-0144.1>.
- Otkin, J.A., Anderson, M.C., Hain, C.R., Svoboda, M., 2014. Examining the relationship between drought development and rapid changes in the evaporative stress index. *Am. Meteorol. Soc.* 15, 938–956. <https://doi.org/10.1175/JHM-D-13-0110.1>.
- Ribeiro da Luz, B., 2006. Attenuated total reflectance spectroscopy of plant leaves: a tool for ecological and botanical studies. *New Phytol.* 172, 305–318. <https://doi.org/10.1111/j.1469-8137.2006.01823.x>.
- Ribeiro Da Luz, B., Crowley, J.K., 2007. Spectral reflectance and emissivity features of broad leaf plants: prospects for remote sensing in the thermal infrared (8.0–14.0 μm). *Remote Sens. Environ.* 109, 393–405. <https://doi.org/10.1016/j.rse.2007.01.008>.
- Ribeiro Da Luz, B., Crowley, J.K., 2010. Identification of plant species by using high spatial and spectral resolution thermal infrared (8.0–13.5 μm) imagery. *Remote Sens. Environ.* 114, 404–413. <https://doi.org/10.1016/j.rse.2009.09.019>.
- Rock, G., Gerhards, M., Schlerf, M., Hecker, C.A., Udelhoven, T., Schlerf, M., Werner, W., Udelhoven, T., 2016. Plant species discrimination using emissive thermal infrared imaging spectroscopy. *Int. J. Appl. Earth Obs. Geoinf.* 53, 16–26. <https://doi.org/10.1016/j.jag.2016.08.005>.
- Salisbury, J.W., 1986. Preliminary measurements of leaf spectral reflectance in the 8–14 μm region. *Int. J. Remote Sens.* 7, 1879–1886.
- Salisbury, J.W., Milton, N.M., 1988. Thermal infrared (2.5 to 13.5 μm) direction hemispherical reflectance of leaves. *Photogramm. Eng. Remote. Sens.* 54, 1301–1304.
- Sepulcre-Cantó, G., Zarco-Tejada, P.J., Jiménez-Muñoz, J.C., Sobrino, J.A., De Miguel, E., Villalobos, F.J., 2006. Detection of water stress in an olive orchard with thermal remote sensing imagery. *Agric. For. Meteorol.* 136, 31–44. <https://doi.org/10.1016/j.agrformet.2006.01.008>.
- Singh, R.P., Roy, S., Kogan, F., 2003. Vegetation and temperature condition indices from NOAA AVHRR data for drought monitoring over India. *Int. J. Remote Sens.* 24, 4393–4402. <https://doi.org/10.1080/0143116031000084323>.
- Snyder, W.C., Wan, Z., 1998. BRDF models to predict spectral reflectance and emissivity in the thermal infrared. *IEEE Trans. Geosci. Remote Sens.* 36, 214–225. <https://doi.org/10.1109/36.655331>.
- Ullah, S., Schlerf, M., Skidmore, A.K., Hecker, C., 2012a. Identifying plant species using mid-wave infrared (2.5–6 μm) and thermal infrared (8–14 μm) emissivity spectra. *Remote Sens. Environ.* 118, 95–102. <https://doi.org/10.1016/j.rse.2011.11.008>.
- Ullah, S., Skidmore, A.K., Naeem, M., Schlerf, M., 2012b. An accurate retrieval of leaf water content from mid to thermal infrared spectra using continuous wavelet analysis. *Sci. Total Environ.* 437, 145–152.
- Ullah, S., Skidmore, A.K., Groen, T.A., Schlerf, M., 2013. Evaluation of three proposed indices for the retrieval of leaf water content from the mid-wave infrared (2–6 μm) spectra. *Agric. For. Meteorol.* 171–172, 65–71.
- Ullah, S., Skidmore, A.K., Ramoelo, A., Groen, T.A., Naeem, M., Ali, A., 2014. Retrieval of leaf water content spanning the visible to thermal infrared spectra. *ISPRS J. Photogramm. Remote Sens.* 93, 56–64. <https://doi.org/10.1016/j.isprsjprs.2014.04.005>.
- Verhoef, W., Jia, L., Xiao, Q., Su, Z., 2007. Unified optical-thermal four-stream radiative transfer theory for homogeneous vegetation canopies. *IEEE Trans. Geosci. Remote Sens.* 45, 1808–1822. <https://doi.org/10.1109/TGRS.2007.895844>.
- Wong, C., Blevin, W., 1967. Infrared reflectances of plant leaves. *Aust. J. Biol. Sci.* 20, 501. <https://doi.org/10.1071/B9670501>.
- Young, S.J., Johnson, R., Hackwell, J.A., 2002. An in-scene method for atmospheric compensation of thermal hyperspectral data. *J. Geophys. Res.* 107, ACH 14-1–ACH 14-20. <https://doi.org/10.1029/2001JD001266>.